Am J Cancer Res 2026;16(4):1589-1607
www.ajcr.us /ISSN:2156-6976/ajcr0172075

Original Article

OTX1 promoting osteosarcoma malignancy by activating PTGS2 transcription

Guangjian Bai[1*], Zhao Li[1*], Zhongfei Huang[2*], Jian Cui[3], Baoquan Xin[3], Zhitao Han[4], Xinghai Yang[3], Tielong Liu[3]

[1]University of Shanghai for Science and Technology, School of Health Science and Engineering, Shanghai, China; [2]Department of Orthopedics, Ruikang Hospital Affiliated to Guangxi University of Chinese Medicine, Nanning, Guangxi, China; [3]Department of Orthopaedic Oncology, The Second Affiliated Hospital of Naval Medical University, Shanghai, China; [4]School of Integrated Chinese and Western Medicine, Nanjing University of Chinese Medicine, Nanjing, Jiangsu, China. [*]Equal contributors and co-first authors.

Received February 12, 2026; Accepted April 22, 2026; Epub April 25, 2026; Published April 30, 2026

Abstract: Osteosarcoma (OS) represents a highly aggressive bone malignancy characterized by limited therapeutic options, particularly in patients presenting with metastasis or recurrence. While the transcription factor Orthodenticle homeobox 1 (OTX1) has been implicated in various cancers, its functional role and underlying mechanism in OS remain largely unknown. In this study, the expression level of OTX1 was examined in OS tissues and cell lines. Aberrant upregulation of OTX1 was observed in OS, and this expression pattern was significantly correlated with unfavorable prognosis in patients. Functional assays revealed that OTX1 overexpression enhanced the proliferation, migration, and invasion abilities of OS cells. Mechanistic studies revealed that OTX1 acts as a transcriptional regulator, activating Prostaglandin-endoperoxide synthase 2 (PTGS2) expression. The upregulation of PTGS2 subsequently mediated anti-apoptotic and pro-invasive phenotypes. Moreover, intervention with the PTGS2 inhibitor celecoxib counteracted the tumor-promoting functions of OTX1 and demonstrated tumor-suppressive effects in in vivo OS models. Herein, results demonstrate that OTX1 drives OS malignant progression by transcriptionally activating PTGS2, which in turn modulates apoptosis- and invasion-related molecules. Targeting the OTX1/PTGS2 axis may represent a promising therapeutic strategy for OS, particularly in high-risk patients with aberrant OTX1 expression.

Keywords: Osteosarcoma, OTX1, PTGS2/COX-2, apoptosis, invasion

Introduction

OS is the most common primary malignant bone tumor, predominantly affecting children and adolescents. Currently, the standard treatment combining neoadjuvant chemotherapy with surgical resection has increased the 5-year survival rate to 60%-70% for patients with localized disease [1]. However, over the past four decades, this survival rate has plateaued without substantial improvement. Approximately 30%-35% of initially localized patients eventually experience recurrence, and the long-term survival rate persists below 30% following the onset of metastasis or recurrence [2]. Numerous clinical trials exploring intensified chemotherapy or novel agents have failed to fundamentally alter this dilemma [3-6]. Therefore, identifying key molecules that drive OS malignancy has emerged as an important research direction to break through the current therapeutic bottleneck and improve patient prognosis.

Transcription factors play a central regulatory role in tumor biology, where they modulate downstream gene networks to influence multiple malignant phenotypes such as cell proliferation, differentiation, apoptosis, invasion, and metastasis. In OS, aberrant expression of various transcription factors has been demonstrated to be closely associated with tumor progression. For example, as a key regulator of osteogenic differentiation, Runt-related transcription factor 2 (RUNX2) promotes OS cell proliferation and metastasis when overexpressed [7], while AP-1 family members such as c-Fos and c-Jun participate in OS tumorigenesis by activating

https://doi.org/10.62347/UULJ3479

multiple oncogenic genes [8, 9]. Moreover, certain Homeobox family transcription factors, including members of the HOXD family, have been found to be dysregulated in OS and linked to altered patient prognosis [10]. These findings suggest that dysregulation of the transcriptional regulatory network constitutes an important component in OS pathogenesis.

OTX1, an important member of the Homeobox family, holds considerable significance in embryonic development, particularly in the formation of the brain and sensory organs [11]. Notably, OTX1 is aberrantly reactivated in various adult malignancies and functions as an oncogene. Studies have shown that in gliomas, elevated OTX1 expression correlates with advanced tumor grade and reduced patient survival [12]. Furthermore, OTX1 enhances tumor invasiveness through the promotion of epithelial-mesenchymal transition. In hepatocellular carcinoma and gastric cancer, OTX1 has also been demonstrated to drive tumor cell proliferation and metastasis by regulating related signaling pathways [13, 14]. These findings establish OTX1 as a pro-oncogenic transcription factor across multiple cancer types. However, the expression profile, biological functions, and specific molecular mechanisms of OTX1 in OS remain poorly elucidated.

Building upon this background, the present study aimed to investigate the oncogenic role of OTX1 in OS and delve into its underlying mechanisms. Experimental results demonstrate that OTX1 binds to the PTGS2 promoter to activate its transcription. Concurrently, elevated PTGS2 expression is associated with enhanced tumor invasiveness and the suppression of apoptotic processes. Overall, this novel discovery provides mechanistic insights into OS malignant progression and lays the groundwork for prognostic assessment and targeted therapeutic strategies in OS.

Materiais and methods

Clinical samples

A total of 56 paired tumor tissues and matched adjacent normal tissues were collected from OS patients at Shanghai Changzheng Hospital (Shanghai, China). All tissues were pathologically confirmed as OS. Following surgical resection, samples were immediately snap-frozen in liquid nitrogen and stored at -80°C or were paraffin-embedded. Clinical and pathological data were extracted from electronic medical records. All patients provided written informed consent prior to participation. The study was approved by the Medical Ethics Committee of Shanghai Changzheng Hospital (No. 2019-SY116, June 16th 2019) and conducted in accordance with the Declaration of Helsinki.

Western blot

Total protein was extracted using RIPA lysis buffer. Proteins were separated by SDS-PAGE and transferred onto PVDF membranes. The membranes were blocked with 5% BSA at room temperature for 1 h, followed by incubation with primary antibodies at 4°C overnight. After three washes with TBST (10 min each) at room temperature, the membranes were incubated with secondary antibody at 37°C for 2 h. Protein bands were visualized by applying chemiluminescence substrate (Thermo Fisher) and detected using an ECL imaging system. All experiments were performed in triplicate. The primary antibodies used in this study were as follows: antibodies against OTX1 (Proteintech, Cat# 26595-1-AP, 1:600), β-Tubulin (Santa Cruz Biotechnology, Cat# sc-5274, 1:1000), IgG (Proteintech, Cat# 80015-1-RR, 1:5000), Lamin B (RayBiotech Cat# 130-10954-500, 1:1000), PTGS2 (Abnova, Cat# H00005743-B01P, 1:1000), Bcl-2 (RayBiotech, Cat# 102-12182, 1:1000), Bax (Abcam, Cat# 182733, 1:2000), caspase-3 (Selleck, Cat# F1080, 1:5000), cleaved caspase-3 (Selleck, Cat# F0135, 1:1000), MMP2 (RayBiotech, Cat# 144-62019-20, 1:500), MMP9 (Antibodies Incorporated, Cat# 75-100, 1:1000), TIMP2 (Proteintech, Cat# 83938-3-RR, 1:5000), and GAPDH (Proteintech, Cat# 60004-1-Ig, 1:50000). Secondary antibodies were acquired from Proteintech (Cat# SA00001-17, 1:6000 and Cat# RGAM001, 1:20000) (horseradish peroxide-conjugated).

Immunofluorescence (IF)

The tissue slices were treated with EDTA buffer for antigen repair and subsequently blocked with 3% BSA. Anti-OTX1 and anti-PTGS2 primary antibodies were applied dropwise to the sections, and they were then incubated at 4°C overnight, followed by treatment with the matching secondary antibody and incubation

for 1 h at normal temperature. Immunofluorescence was detected by a three-colour fluorescence kit (Shanghai Recordbio Biological Technology, Shanghai, China). Then, DAPI was used to stain the nucleus. The images were observed and collected under an inverted micro-scope. The nucleus is dyed blue by DAPI, OTX1 is coloured red, and PTGS2 is coloured green.

Quantitative real-time PCR (qRT-PCR)

RNA extraction from the tissue samples was performed by homogenization. Briefly, tissue samples were cut into fragments and transferred into 2 ml tubes, followed by the addition of TRIzol (1 ml) to each tube. The samples were then subjected to homogenization, and the supernatant was collected. The following steps were performed according to the instructions for TRIzol (Invitrogen Corporation, 15596-018). For reverse transcription, we utilized the Evo M-MLV RT Premix for qPCR kit. The reaction mixture (20 µl) contained 1 µg of total RNA, 4 µl of 5× Evo M-MLV RT Premix, and RNase-free water up to 20 µl. The reaction was carried out at 37°C for 15 min, followed by 85°C for 5 sec to inactivate the enzyme. Subsequent qPCR was performed using the SYBR Green Premix Pro Taq HS qPCR kit. Each 20 µl reaction contained 10 µl of 2× SYBR Green Premix Pro Taq HS, 0.4 µl each of forward and reverse primers (10 µM), 2 µl of cDNA template (diluted 1:5), and 7.2 µl of RNase-free water. The qPCR program was as follows: initial denaturation at 95°C for 30 s; followed by 40 cycles of 95°C for 15 s (denaturation), 58°C for 20 s (annealing), and 72°C for 30 s (extension); fluorescence signal was acquired during the extension step. After amplification, a melting curve analysis was performed from 60°C to 95°C with a temperature increment of 0.5°C every 5 s to verify product specificity. β-Tubulin was used as an internal control. All qPCRs were conducted on a 7900HT Fast Real-Time PCR System. Supplementary Table 1 lists the primers used.

Cell culture

All cell lines cultured in this study were obtained from American Type Culture Collection (ATCC) and were cultured following the instructions from ATCC. hFOB 1.19 and MG63, 143B, HOS, and Saos-2 cells were cultured in DMEM with 10% foetal bovine serum (FBS) and 1% penicillin-streptomycin supplements at 37°C and 5% CO_2 in a humidified atmosphere. Plasmids and siRNAs were purchased from Shanghai GeneChem (Shanghai, China). A density of 2×10^5 cells/well was used for culturing OS cells. All cell lines were authenticated by short tandem repeat analysis and confirmed to be Mycoplasma-free.

Lentivirus packaging and infection

For lentivirus-related experiments, we transfected HEK293T cells with the appropriate lentiviral expression vector (pLVX-IRES-Puro-OTX1 or pLKO.1-sh-OTX1-1/2) and packaging plasmids (psPAX2 and pMD2.G) using Lipofectamine 3000 transfection reagent. Each virus-containing supernatant was collected 48 h upon transfection and infected with the target cells (143B and HOS) at 70% confluence. Besides, 1 µg/mL puromycin was employed for drug-based selection for one week.

Cell counting kit-8 assay (CCK-8)

Cell proliferation was assessed using the CCK-8 (APExBIO, USA). Transfected HOS and 143B cells were seeded in 96-well plates (1,000 cells/well) and incubated for 0, 24, 48, 72 hours. CCK-8 reagent was added to each well, and absorbance was measured at 450 nm.

5-Ethynyl-2'-deoxyuridine assay (EdU)

EdU incorporation was detected using the EdU Cell Proliferation Kit (Beyotime, China). Cells were incubated with EdU (50 µM) for 2 hours, fixed with 4% paraformaldehyde, permeabilized with 1% Triton X-100, and stained with Azide594 and Hoechst 33342. Fluorescence signals were visualized by confocal microscopy.

Wound healing assay

Cells were seeded in 6-well plates and cultured until they reached approximately 90% confluence. A uniform, straight scratch was then created across the cell monolayer using a sterile 200 µL pipette tip. The detached cells and debris were removed by gently washing twice with pre-warmed phosphate-buffered saline (PBS). Subsequently, the cells were incubated

in low-serum medium (containing 0.5% fetal bovine serum) to minimize proliferation effects while allowing migration. To track the same field over time, reference marks were made on the bottom of each well. Images of the wound area were captured at 0, 12, and 24 hours using microscope. The migration rate was quantified by measuring the reduction in wound width using ImageJ software.

Transwell assay

In a 24-well plate, the cell invasion assay was carried out. Cell migration was assessed using Transwell chambers (8-μm pore). 5×10^4 cells in 200 μL serum-free medium were seeded into the upper chamber, while the lower chamber contained 600 μL complete medium with 10% FBS as a chemoattractant. After 24 h of incubation, non-migrated cells on the upper membrane surface were removed with a cotton swab. Cells on the lower surface were fixed with 4% paraformaldehyde, washed with PBS, stained with 0.1% crystal violet, and rinsed again. After air-drying, migrated cells were quantified by counting five random fields per membrane under an inverted microscope.

Luciferase reporter assay

The putative promoter region of the target gene was cloned into the pGL3-Basic vector to generate the firefly luciferase reporter plasmid. Cells (HEK293T) were co-transfected with this reporter plasmid, an OTX1-overexpression or control plasmid, and a Renilla luciferase plasmid (pRL-TK) as an internal control for normalization. After 24-48 h of incubation, cells were lysed, and firefly and Renilla luciferase activities were measured sequentially using a dual-luciferase reporter assay system on a microplate luminometer. The relative promoter activity was expressed as the ratio of firefly to Renilla luciferase luminescence. Each experiment was performed in triplicate and repeated at least three times independently.

Flow cytometry

Cells were seeded in 6-well plates at a density of 2×10^5 cells per well and treated with staurosporine (1 μM) for 24 h. After treatment, cells were harvested, washed with cold PBS, and resuspended in 1× binding buffer. The cells were then stained with Annexin V-FITC and PI for 15 min at room temperature in the dark. Subsequently, 400 μL of binding buffer was added, and the samples were analyzed on a BD Accuri C6 flow cytometer. A minimum of 10,000 events were recorded per sample, and apoptotic cells were quantified as the percentage of Annexin V-positive cells using FlowJo software (version 10.8.1).

Chromatin immunoprecipitation followed by polymerase chain reaction (ChIP-PCR)

Cells were crosslinked with 1% formaldehyde, and chromatin was sheared to 200-1000 bp by sonication. After pre-clearing, soluble chromatin was incubated overnight at 4°C with specific antibody or control IgG, followed by capture with Protein A/G beads. Beads were washed sequentially with low-salt, high-salt, LiCl, and TE buffers. Bound complexes were eluted, crosslinks were reversed, and DNA was purified. Target genomic regions were amplified by PCR, and enrichment was calculated relative to Input and control samples. The related Primers sequences are listed in Supplementary Table 1.

Enzyme-linked immunosorbent assay (ELISA)

Briefly, after collecting the conditioned media from each group (OTX1-overexpress, OTX1-knockdown and vector), cell debris was removed by centrifugation at 3000 rpm for 10 minutes at 4°C. A commercial PGE2 ELISA kit (Solarbio, SEKH-0414) was employed according to the manufacturer's instructions. 100 μL of standard dilutions or samples were added to the 96-well plate pre-coated with anti-PGE2 antibody and incubated for 2 hours at room temperature. After washing, a biotinylated detection antibody was added for 1 hour, followed by incubation with horseradish peroxidase-conjugated streptavidin for 30 minutes. The signal was developed using tetramethylbenzidine (TMB) substrate for 15-30 minutes in the dark, and the reaction was stopped with 2 M H_2SO_4. The absorbance was read at 450 nm with a reference wavelength of 570 nm. PGE2 concentrations were calculated from a standard curve generated using serial dilutions of the provided standard, and the values were normalized to total cell number or total protein content.

RNA sequencing (RNA-seq)

RNA was isolated using TRIzol reagent, and library construction was performed following standard protocols. Sequencing was carried out on the BGISEQ-500 platform (BGI, China). For gene expression analysis, reads were normalized to FPKM (Fragments Per Kilobase of transcript per Million mapped reads). Genes with a fold change ≥ 2 and a false discovery rate (FDR) < 0.001 were defined as significantly differentially expressed. Gene Ontology (GO) enrichment analysis was conducted using the corresponding R package with these significant genes as input.

In vivo study

Eight-week-old female Balb/c nude mice were purchased from the Animal Center of Shanghai Institute of Cell Biology (Shanghai, China). Animals in each group received an orthotopic injection into the tibial plateau with 143B cells (5×10^6 cells suspended in 100 μL PBS) of distinct genetic backgrounds: empty vector (Vector), OTX1-knockdown (OTX1-Sh), and OTX1-overexpress (OTX1-OE). Tumor growth was monitored every three days starting from day 7 post-injection using a vernier caliper. Tumor volume was calculated according to the formula: Volume = 0.52 × length × width. Mice in the treatment group were administered celecoxib (25 mg/kg/day) via oral gavage for two weeks. At the experimental endpoint, all mice were euthanized by CO_2 inhalation. Tumors were excised, weighed, and photographed for further analysis. All animal procedures were performed in accordance with institutional animal welfare guidelines and approved by the Institutional Animal Care and Use Committee (IACUC) of Jiangsu Aniphe Biolaboratory Inc (Approval No. 2023SY106; Date: October 11, 2023).

Statistics

Statistical analyses were performed using GraphPad Prism 7.0. All values are reported as the mean ± standard deviation (SD). Differences between groups were analyzed by one-way or two-way ANOVA, the Kaplan-Meier method and log-rank test were used to compare survival curves and determine statistical significance, respectively. For CCK-8 assay and in vivo tumor volume measurement, a two-way repeated measures ANOVA was performed, with group as the between-subject factor and time as the within-subject factor. When a significant group × time interaction was detected, simple effects analysis was conducted using Bonferroni-corrected post-hoc tests to compare groups at each time point. Greenhouse-Geisser correction was applied when the sphericity assumption was violated. A P value < 0.05 was regarded as statistically significant.

Results

OTX1 upregulation correlates with poor prognosis in OS

To determine the expression profile of OTX1 in OS, OTX1 mRNA and protein levels in 24 pairs of OS were initially detected, and adjacent normal tissues were matched by qRT-PCR and Western blot. Results revealed that OTX1 expression was remarkably upregulated in OS tissues compared with adjacent normal tissues (**Figure 1A**, **1B**). Subsequently, in situ immunohistochemical (IHC) staining was performed to assess OTX1 protein expression in 56 OS samples, and the staining intensity was recorded for each sample. Based on the immunohistochemical score of OTX1, these 56 OS samples were further divided into the high-expression group (++ and +++) and the low-expression group (negative and +) (**Figure 1C**). Clinicopathological correlation analysis demonstrated that elevated OTX1 expression was significantly associated with lower overall survival and progression-free survival rates (**Figure 1D**, **1E**). Collectively, these results indicate that OTX1 is aberrantly upregulated in OS and exhibits an inverse correlation with patient prognosis.

OTX1 overexpression promotes OS cell proliferation, migration, and invasion

Herein, OTX1 expression was detected in human osteoblast cells (hFOB 1.19) and OS cell lines (including MG63, 143B, HOS, and Saos-2). Results revealed significantly increased OTX1 levels in OS cell lines (MG63, 143B, HOS, and Saos-2) compared with hFOB 1.19 (**Figure 2A**). To determine the function of OTX1 in OS, OTX1 in HOS and 143B cells was stably overexpressed or knocked down via lentiviral infection, as confirmed by Western blotting (**Figure 2B**, **2C**). Subsequently, the

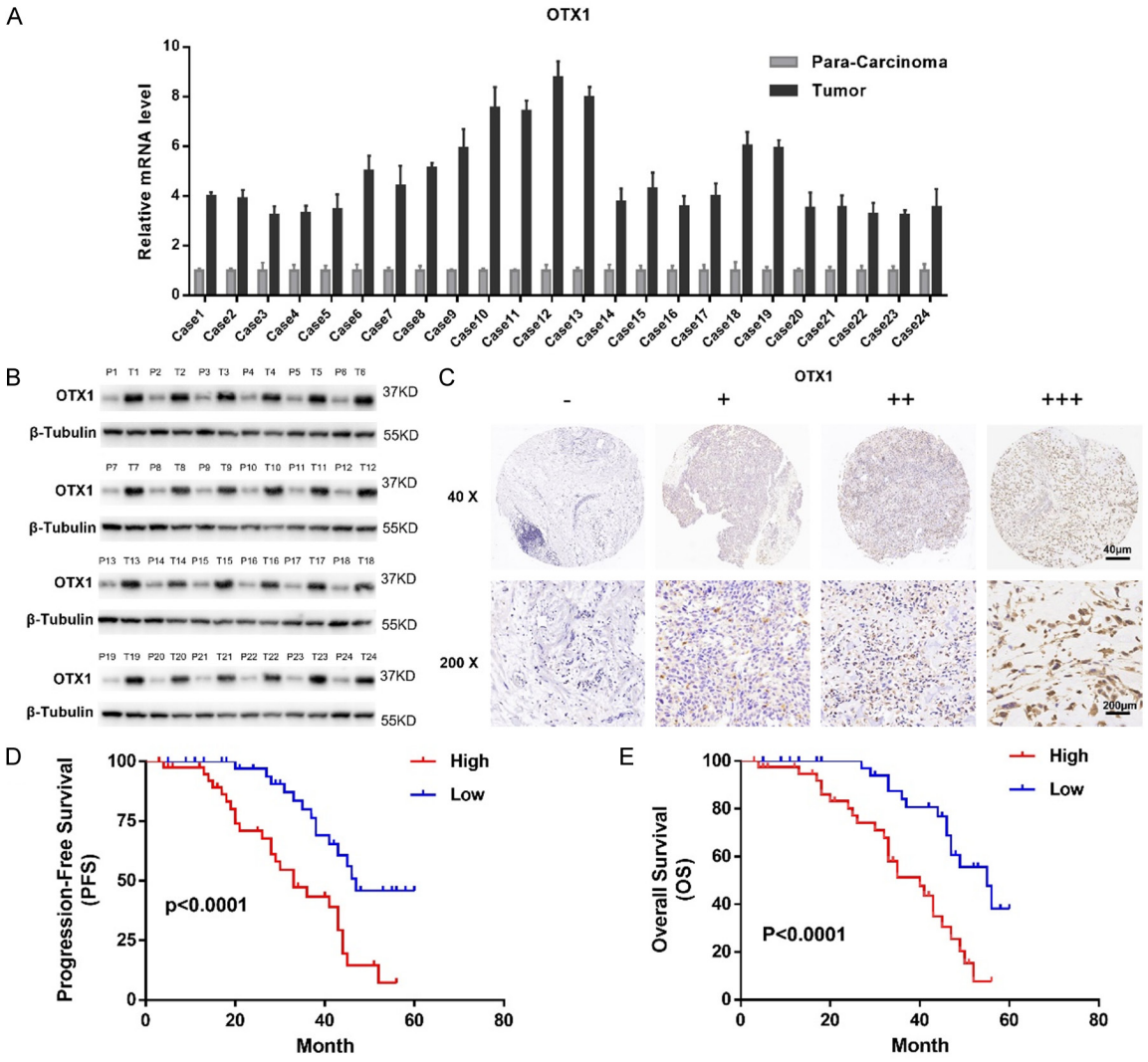

Figure 1. OTX1 upregulation correlates with poor prognosis in OS. A, B. OTX1 mRNA and protein levels in OS and adjacent tissues by qRT-PCR and Western blot. C. Five-micrometer (5-μm) sections analyzed by IHC using anti-OTX1 antibodies. Quantitative analyses (Negative and + = low expression, ++ and +++ = high expression) were performed for each sample. D. Kaplan-Meier curve showing the correlation between OTX1 expression levels and recurrence-free survival rate in OS patients. E. Kaplan-Meier curve showing the correlation between OTX1 expression levels and overall survival in OS patients. Statistical analysis was performed using one-way ANOVA. Scale bars, 40 μm or 200 μm.

effect of OTX1 on OS proliferative activity was evaluated using CCK-8 and EdU assays. Results indicated that OTX1 overexpression enhanced the proliferative activity of OS cells, whereas OTX1 knockdown suppressed the proliferation (**Figure 2D-F**). Additionally, the impact of OTX1 on OS cell migration and invasion was assessed by wound healing and Transwell assays, confirming that OTX1 knockdown inhibited the migration and invasion abilities of OS, while OTX1 overexpression notably promoted these capabilities (**Figure 2G**, **2H**).

OTX1 activates PTGS2 transcription in OS cells

To clarify the molecular mechanism underlying OTX1-mediated promotion of OS development, this study transfected 143B cells with either the pcDNA3.1-OTX1 overexpression vector or an empty control vector and performed transcriptome sequencing analysis. Differential expression analysis identified 629 significantly up- or down-regulated genes (**Figure 3A**, **3B**). GO enrichment analysis indicated that these differential genes were primarily involved in bio-

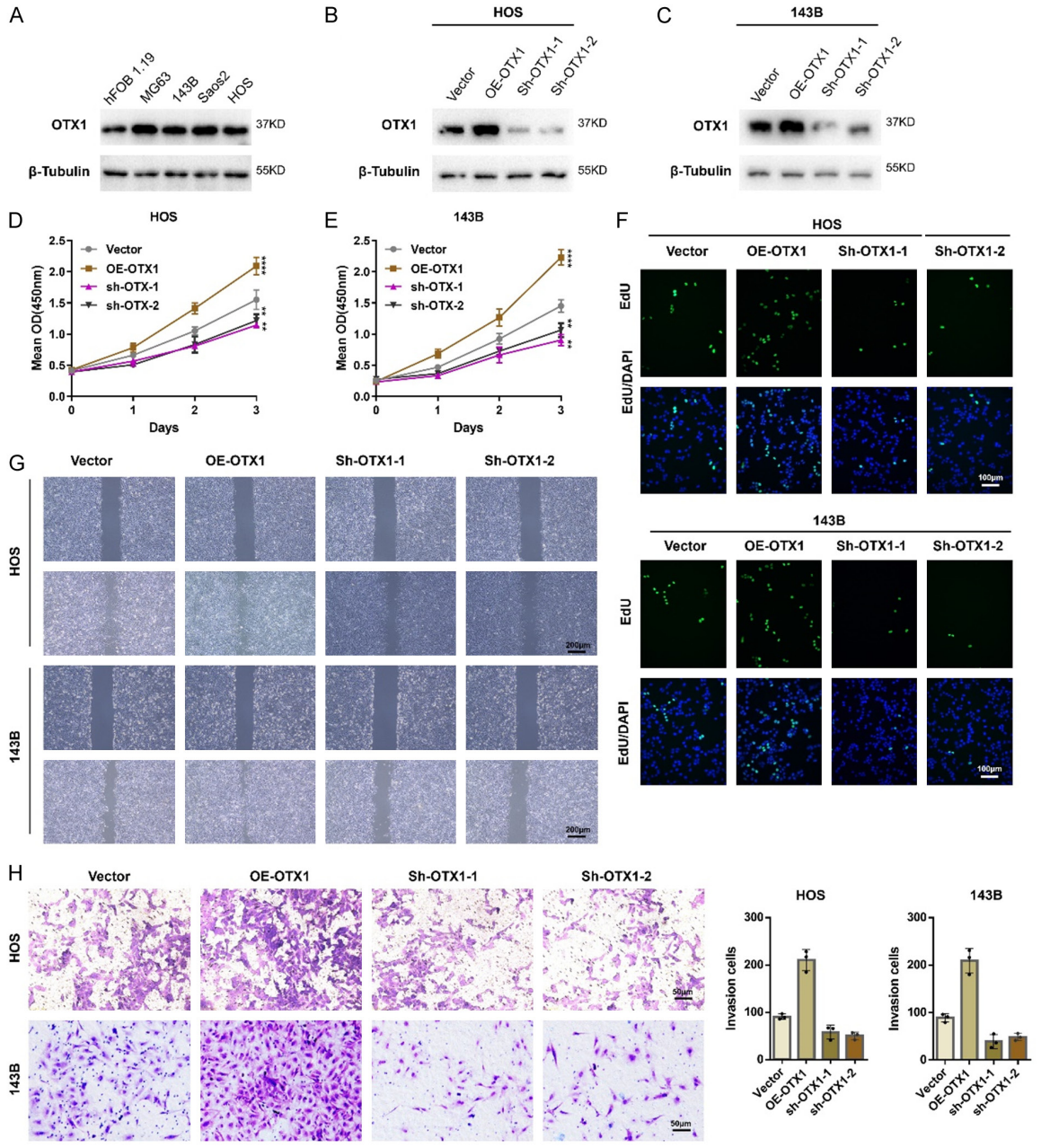

Figure 2. OTX1 overexpression promotes OS cell proliferation, migration, and invasion. (A) OTX1 protein levels in OS cell lines (MG63, 143B, Saos-2, and HOS) and hFOB 1.19 by Western blot. (B, C) Protein expression of OTX1 gain and loss in 143B and HOS cells validated by western blot. (D, E) CCK8 assays performed to evaluate the proliferation activity of the indicated OS cells with OTX1 overexpression or knockdown. (F) EdU assay performed to assess the effects of OTX1 on the proliferative activity of indicated OS cells. (G) Wound healing assays performed to evaluate the effect of OTX1 on the migration of the indicated OS cells. (H) Transwell assays performed to evaluate the effects of OTX1 on the migration of the indicated OS cells. Statistical analysis were performed using two-way repeated measures ANOVA with Bonferroni's post-hoc test (D, E) and two-way ANOVA (H). Error bars show means ± SD. *P < 0.05, **P < 0.01; ***P < 0.001, ****P < 0.0001. Scale bars, 50 μm, 100 μm and 200 μm.

logical processes such as "collagen-containing extracellular matrix", "response to virus", and "defence response to virus" (**Figure 3C**). Further screening revealed that no gene was down-regulated by more than 4-fold, whereas two genes, PTGS2 and Alkaline phosphatase, placental (ALPP), were up-regulated by more than 4-fold (**Figure 3D**). This suggested that both

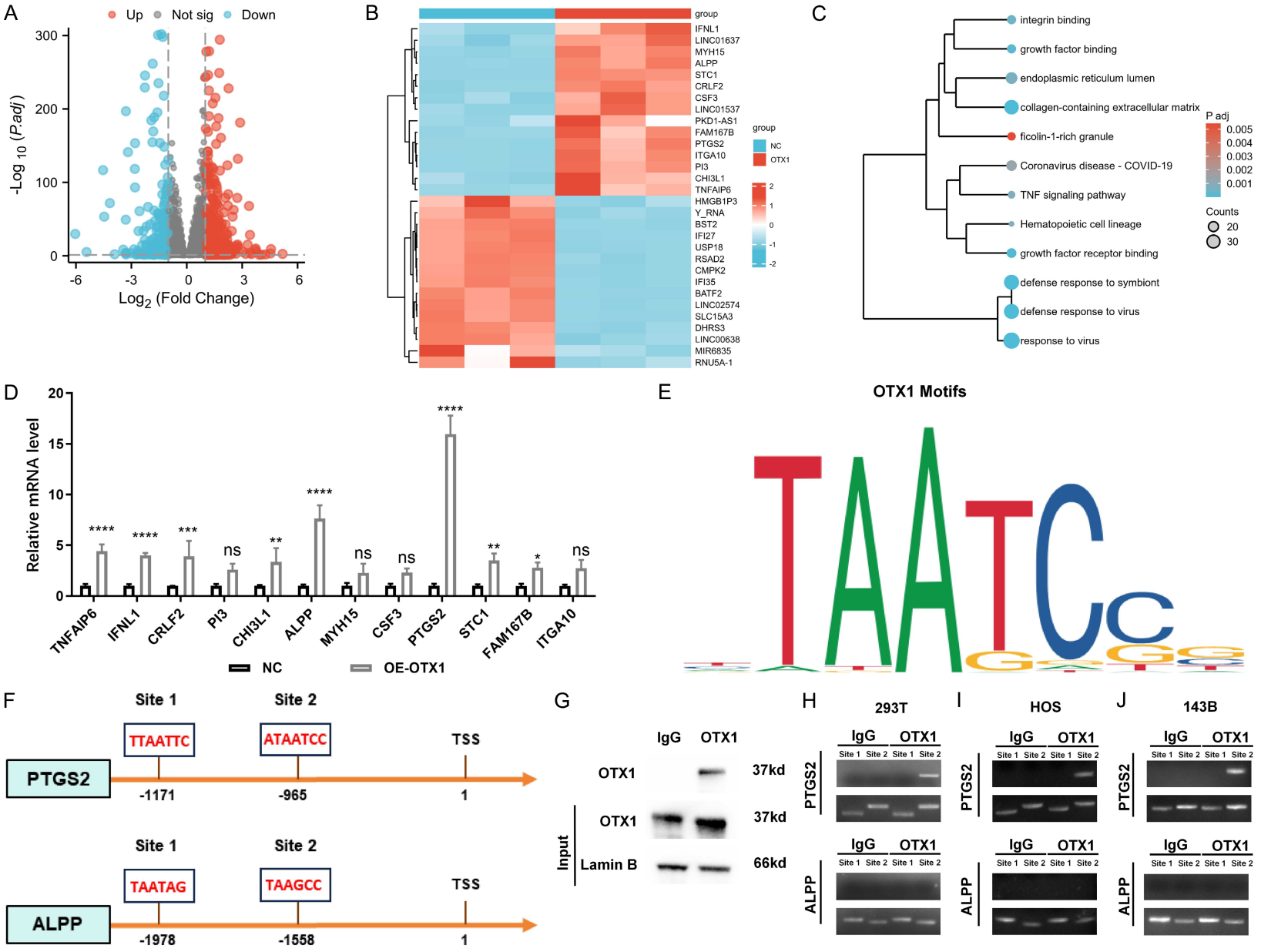
A
Up
Not sig
Down
-Log 10 (P.adj)
Log2 (Fold Change)
B
group
IFNL1
LINC01637
MYH15
ALPP
STC1
CRLF2
CSF3
LINC01537
PKD1-AS1
FAM167B
PTGS2
ITGA10
PI3
CHI3L1
TNFAIP6
HMGB1P3
Y_RNA
BST2
IFI27
USP18
RSAD2
CMPK2
IFI35
BATF2
LINC02574
SLC15A3
DHRS3
LINC00638
MIR6835
RNU5A-1
NC
OTX1
C
integrin binding
growth factor binding
endoplasmic reticulum lumen
collagen-containing extracellular matrix
ficolin-1-rich granule
Coronavirus disease - COVID-19
TNF signaling pathway
Hematopoietic cell lineage
growth factor receptor binding
defense response to symbiont
defense response to virus
response to virus
P adj
Counts
D
Relative mRNA level
TNFAIP6
IFNL1
CRLF2
PI3
CHI3L1
ALPP
MYH15
CSF3
PTGS2
STC1
FAM167B
ITGA10
NC
OE-OTX1
E
OTX1 Motifs
F
Site 1
Site 2
TSS
PTGS2
TTAATTC
ATAATCC
-1171
-965
1
ALPP
TAATAG
TAAGCC
-1978
-1558
1
G
IgG
OTX1
OTX1
37kd
OTX1
37kd
Input
Lamin B
66kd
H
293T
I
HOS
J
143B
PTGS2
ALPP
Site 1
Site 2

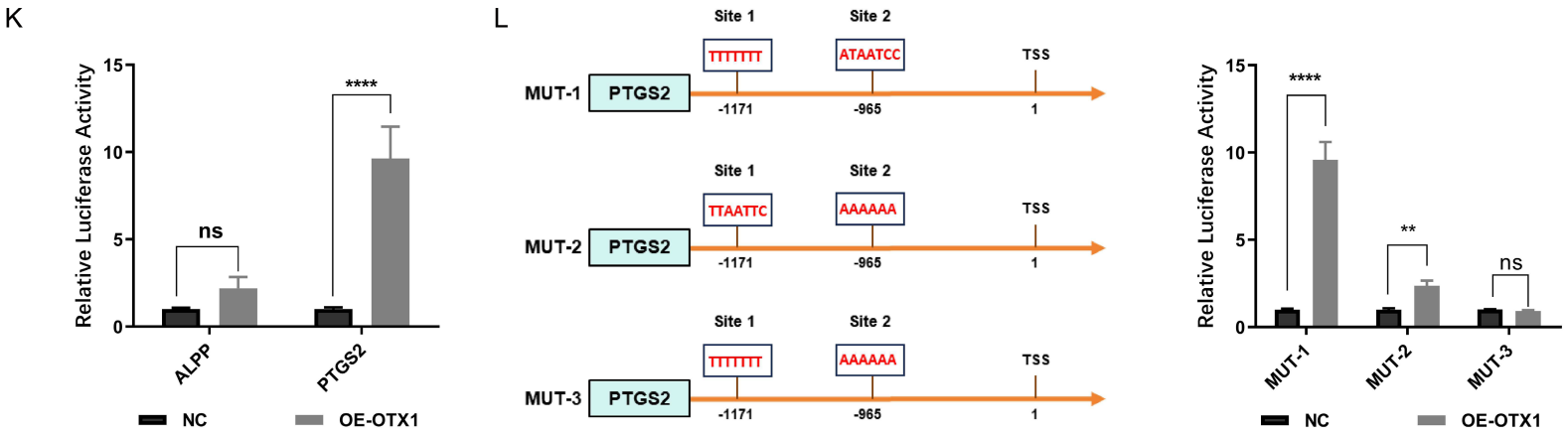

Figure 3. OTX1 activates PTGS2 transcription in OS cells. A, B. RNA sequencing performed in wild-type cells and OTX1 overexpression cells. Difference analysis of the transcriptome sequencing data was performed using the R Statistical Software. C. GO enrichment performed on the differential genes. D. Differentially upregulated genes upon OTX1 overexpression. E, F. Prediction of the OTX1 binding motif within the PTGS2 and ALPP promoter through the JASPAR dataset. G-J. Validation of the OTX1-PTGS2 regulatory relationship by ChIP-PCR. K. Dual-luciferase reporter assay of PTGS2 and ALPP. L. Dual-luciferase assay used to analyze the effect of OTX1 on the PTGS2 promoter with different mutational sites. Statistical analysis was performed using two-way ANOVA. Error bars show means ± SD. NS, not significant; *P < 0.05, **P < 0.01, ***P < 0.001, ****P < 0.0001.

might be transcriptionally regulated by OTX1. To validate this hypothesis, the characteristic binding motif of OTX1 was further retrieved from the JASPAR database, and predictive analysis was performed on the promoter regions (up to 2000 bp upstream of the transcription start site) of PTGS2 and ALPP. Two potential OTX1-binding sites were identified in each promoter (**Figure 3E**, **3F**). Subsequently, ChIP-PCR was conducted in HEK293T cells overexpressing OTX1. Results demonstrated that OTX1 specifically bound to site 2 within the PTGS2 promoter region (**Figure 3G-J**). Moreover, dual-luciferase reporter assays showed that OTX1 could regulate PTGS2 expression, yet exerted no effect on ALPP expression (**Figure 3K**). To further define the binding site of OTX1 within the PTGS2 promoter, a luciferase reporter vector driven by the PTGS2 promoter was constructed, and corresponding mutant vectors were generated. Results showed that OTX1-mediated activation of the reporter gene was significantly reduced only when binding site 2 was mutated (**Figure 3L**), confirming this site as the key region for direct binding and transcriptional activation by OTX1. Collectively, these results establish that OTX1 enhances the transcriptional activity of PTGS2 through direct binding to a specific site in its promoter.

PTGS2 overexpression inhibits apoptosis while promoting migration and invasion in OS cells

PTGS2 (also known as Cyclooxygenase-2, COX-2) matters considerably in tumor development. By catalyzing the conversion of arachidonic acid to prostaglandins - particularly PGE2-it forms a critical inflammatory-oncogenic signaling hub that broadly regulates the expression and activity of apoptosis-related proteins and matrix metalloproteinases (MMPs), thereby promoting tumor cell survival, invasion and metastasis [15, 16]. Building on prior findings confirming OTX1-mediated transcriptional activation of PTGS2, further investigation was hereby conducted to clarify whether PTGS2 mediates OTX1-driven malignant phenotypes in OS. For this purpose, OTX1 was either overexpressed or knocked down in 143B and HOS cells, followed by Western blot analysis of the expression levels of PTGS2, apoptosis-associated proteins (including Bcl-2, Bax, and cleaved caspase-3), MMPs (including MMP2 and MMP9), and the endogenous MMP2 inhibitor Tissue inhibitor of metalloproteinases 2 (TIMP2). Results showed that the Bcl-2/Bax ratio was increased in the PTGS2 overexpression group, with cleaved caspase-3 being barely detectable, indicating an anti-apoptotic state. Regarding invasion and migration related proteins, MMP2 and MMP9 levels were markedly upregulated in the PTGS2-overexpression group, while TIMP2 expression was reduced, suggesting enhanced extracellular matrix-degrading capacity and increased migratory and invasive potential (**Figure 4A**, **4B**).

PGE2 is a key catalytic product of PTGS2. Subsequently, we measured the levels of PGE2 by ELISA in OS cells subjected to OTX1 overexpression or knockdown. The results showed that OTX1 overexpression significantly increased PGE2 levels, whereas OTX1 knockdown decreased PGE2 levels (**Figure 4C**). This pattern fully mirrored the regulatory effect of OTX1 on PTGS2 protein expression, indicating that OTX1 may affect PGE2 generation through modulation of PTGS2 expression. At the functional level, TUNEL apoptosis assays confirmed that PTGS2 overexpression effectively suppressed OS cell apoptosis, whereas PTGS2 knockdown significantly promoted apoptosis (**Figure 4D**, **4E**). Together, these results indicate that PTGS2-mediated inhibition of apoptosis and enhancement of migration and invasion may represent a critical downstream mechanism through which OTX1 drives OS progression.

Inhibiting PTGS2 activity abrogates the oncogenic effects of OTX1

To determine whether PTGS2 mediates the OTX1-driven malignant phenotype in OS, a selective PTGS2 inhibitor (celecoxib) was hereby utilized to pharmacologically suppress PTGS2 activity [17]. Western blot analysis revealed that celecoxib treatment effectively reversed the molecular alterations induced by OTX1 overexpression. Specifically, it abolished the anti-apoptotic effects of OTX1, including the elevated Bcl-2/Bax ratio and the suppression of cleaved caspase-3. Simultaneously, the OTX1-mediated upregulation of MMP2 and MMP9, as well as the downregulation of TIMP2, was also reversed (**Figure 5A**, **5B**). This indicates that inhibiting PTGS2 activity is suffi-

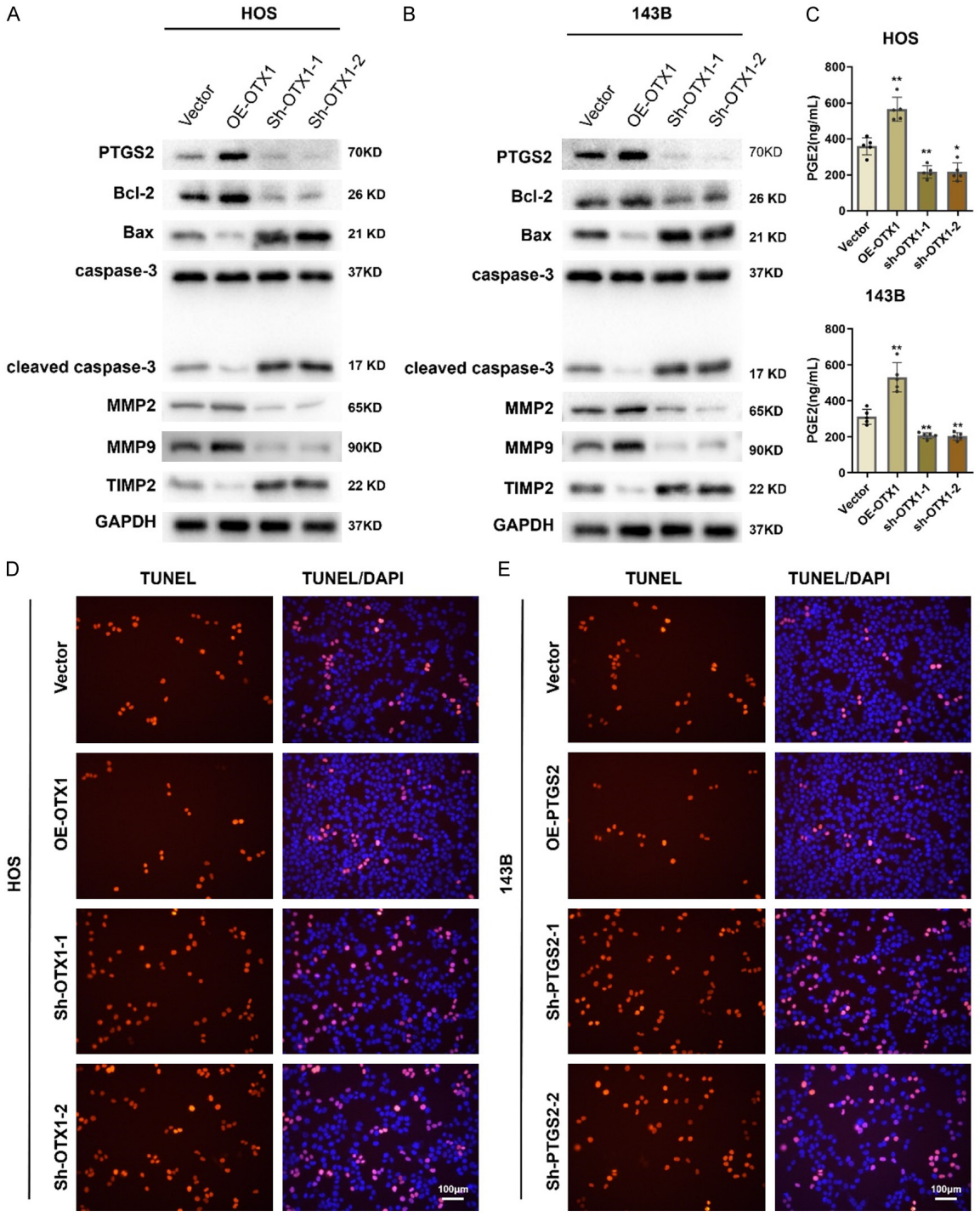

Figure 4. PTGS2 overexpression inhibits apoptosis and promotes migration and invasion in OS cells. A, B. Expression of Bcl-2, Bax, cleaved caspase-3, MMP2, MMP9, and TIMP2 on 143B and HOS cells with OTX1 overexpression or knockdown. C. ELISA assay to detect the effect of OTX1 overexpression and knockdown on PGE2 levels. D, E. TUNEL staining to detect the effect of OTX1 overexpression and knockdown on the apoptosis of OS cells. Statistical analysis were performed using two-way ANOVA. Error bars show means ± SD. *P < 0.05, **P < 0.01. Scale bars, 100 μm.

cient to counteract OTX1's regulation of apoptosis- and invasion-related pathways. At the functional level, CCK-8 assays confirmed that celecoxib significantly attenuated the pro-pro-

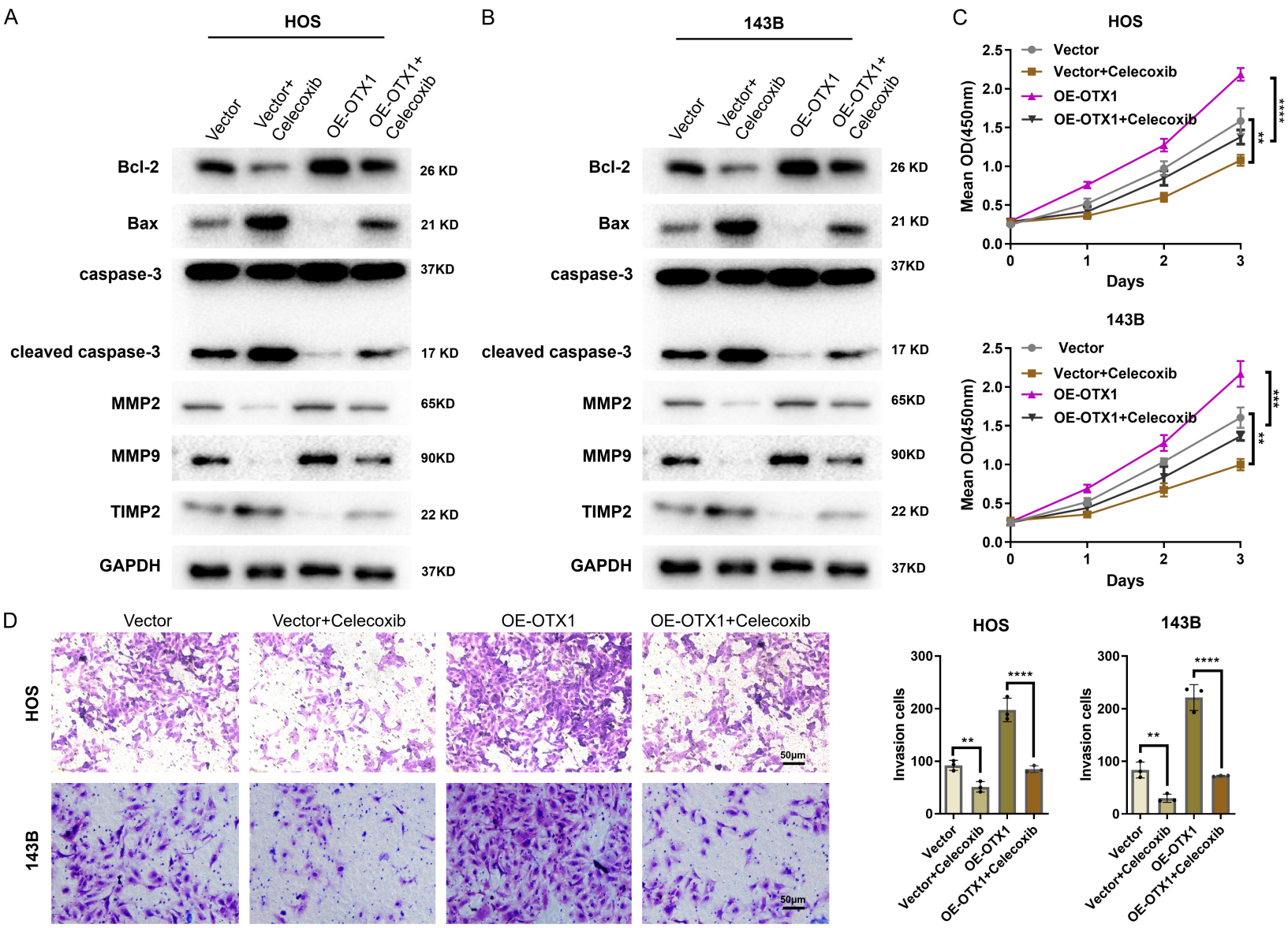
A
HOS
Vector
Vector+ Celecoxib
OE-OTX1
OE-OTX1+ Celecoxib
Bcl-2
26 KD
Bax
21 KD
caspase-3
37KD
cleaved caspase-3
17 KD
MMP2
65KD
MMP9
90KD
TIMP2
22 KD
GAPDH
37KD
B
143B
C
HOS
Vector
Vector+Celecoxib
OE-OTX1
OE-OTX1+Celecoxib
Mean OD(450nm)
Days
143B
D
Vector
Vector+Celecoxib
OE-OTX1
OE-OTX1+Celecoxib
HOS
143B
50μm
Invasion cells

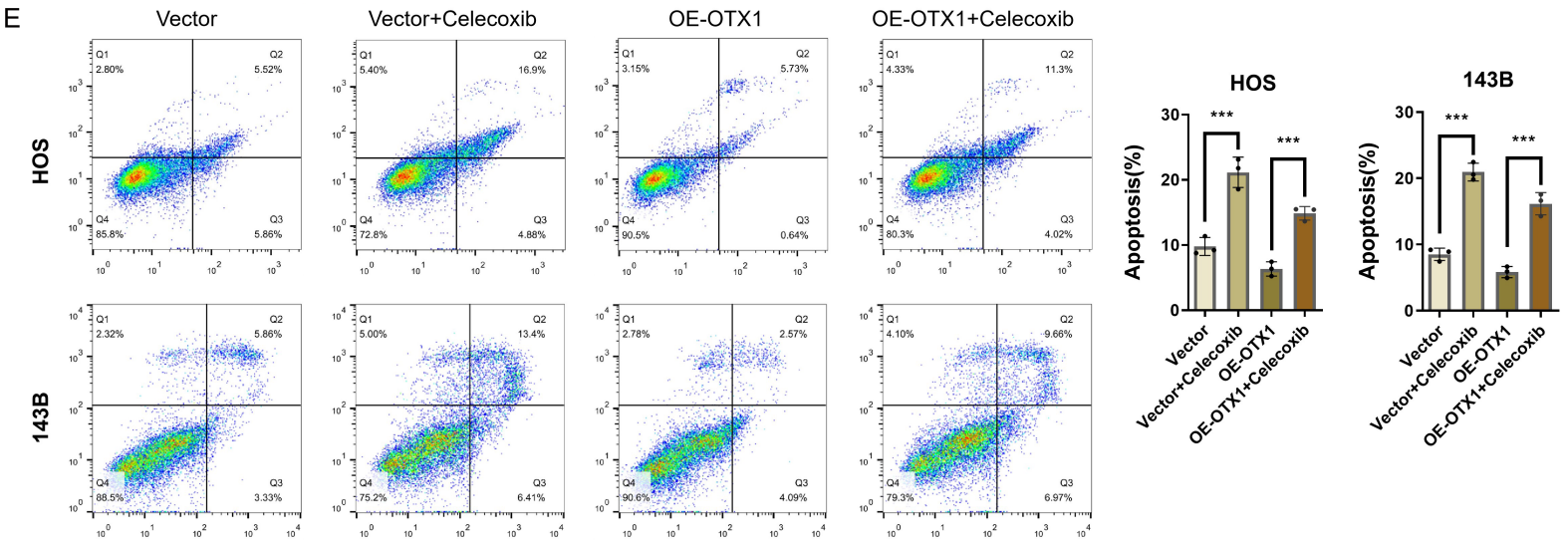

Figure 5. Inhibiting PTGS2 activity abrogates the oncogenic effects of OTX1. (A, B) Western blots performed to detect the expression levels of Bcl-2, Bax, cleaved caspase-3, MMP2, MMP9, and TIMP2 in indicated OS cells. (C) CCK-8 assays performed to evaluate the effects of celecoxib on the proliferation of the indicated OS cells. (D) Transwell assays performed to evaluate the effects of celecoxib on the migration of the indicated OS cells. (E) Flow cytometry assays performed to evaluate the effects of celecoxib on the apoptosis of the indicated OS cells. Statistical analysis were performed using two-way repeated measures ANOVA with Bonferroni's post-hoc test (C) and multifactor ANOVA (D, E). Error bars show means ± SD. **P < 0.01, ***P < 0.001, ****P < 0.0001. Scale bars, 50 μm.

liferative effect of OTX1 on OS cells (**Figure 5C**). Transwell assays further demonstrated that celecoxib treatment reversed the enhanced cell migration and invasion capabilities caused by OTX1 overexpression (**Figure 5D**). Additionally, the direct regulatory role of OTX1 on cell apoptosis was validated using Annexin V-FITC/PI flow cytometry. OTX1 knockdown promoted apoptosis, while OTX1 overexpression inhibited it (**Figure 5E**). This result aligns with the aforementioned PTGS2-mediated anti-apoptotic phenotype. In summary, selective inhibition of PTGS2 activity comprehensively reverses the pro-proliferative, anti-apoptotic, and pro-invasive/migratory effects induced by OTX1 overexpression, further positioning PTGS2 as a critical downstream effector molecule through which OTX1 drives the malignant progression of OS.

To further validate whether PTGS2 is a key effector molecule of OTX1, we performed rescue experiments by overexpressing PTGS2 in OTX1-knockdown OS cells (Supplementary Figure 1A, 1B). The results showed that OTX1 knockdown suppressed cell proliferation and migration, and promoted apoptosis, whereas concomitant overexpression of PTGS2 reversed these effects (Supplementary Figure 1C-G). PTGS2 overexpression alone was sufficient to rescue the phenotypic changes induced by OTX1 knockdown, indicating that PTGS2 serves as a critical downstream mediator of OTX1 in regulating the malignant progression of OS.

OTX1 knockdown or PTGS2 inhibitor suppresses OS growth in vivo

To validate the tumor-promoting role of OTX1 in vivo and evaluate the therapeutic potential of targeting PTGS2, an orthotopic OS xenograft model was further established. Specifically, stable OTX1-knockdown, OTX1-overexpress, and control 143B cells were orthotopically injected into the tibial plateau of BALB/c nude mice. Upon tumor establishment (day 7 post-injection), mice were treated with celecoxib (25 mg/kg/day, oral gavage) for two weeks. Results showed that compared with the control group, both the OTX1-knockdown group and the celecoxib-treated group exhibited significantly slower tumor growth, along with markedly reduced final tumor volume and weight. Notably, celecoxib treatment effectively reversed the tumor-proliferation advantage conferred by OTX1 overexpression (**Figure 6A-C**). To further verify the molecular effects in vivo, Western blot analysis was performed on tumor tissues. Results revealed that PTGS2 protein levels were correspondingly downregulated in OTX1-knockdown tumors (**Figure 6D**). This is consistent with the conclusion that OTX1 transcriptionally regulates PTGS2. Finally, to explore the clinical relevance of this mechanism, multiplex immunofluorescence staining was also conducted for OTX1 and PTGS2 on OS samples. Results uncovered that in tumor tissues, cells positive for OTX1 expression also exhibited high PTGS2 expression, demonstrating a significant co-localization relationship between the two (**Figure 6E**). This suggests that the OTX1/PTGS2 regulatory axis is also operative in human OS. In summary, the present in vivo experiments indicate that both genetic knockdown of OTX1 and pharmacological inhibition of its downstream target PTGS2 effectively suppress OS growth. Combined with the co-expression pattern observed in clinical samples, these findings robustly confirm the critical driving role of the OTX1/PTGS2 signaling axis in OS progression.

Discussion

OS represents a highly aggressive and readily metastatic malignant bone tumor, with the primary challenge in clinical management lying in the effective control of recurrent or metastatic cases. While the current standard of neoadjuvant chemotherapy combined with surgery has improved survival rates among patients with localized disease, the prognosis remains poor for a substantial proportion of patients who develop metastasis or recurrence. Therefore, gaining deeper insights into the drivers of OS progression, particularly identifying key molecules affecting metastatic potential and apoptosis resistance is crucial for developing novel therapeutic strategies and improving patient outcomes. This study provides the first systematic evidence that OTX1 transcriptionally activates PTGS2 (COX-2) to coordinately disrupt apoptosis and extracellular matrix homeostasis, thereby driving the multifaceted malignant progression of OS encompassing proliferation, survival, migration, and invasion (**Figure 7**). This discovery not only provides a novel molecular perspective for understanding the clinical heterogeneity of OS but also forges a crucial

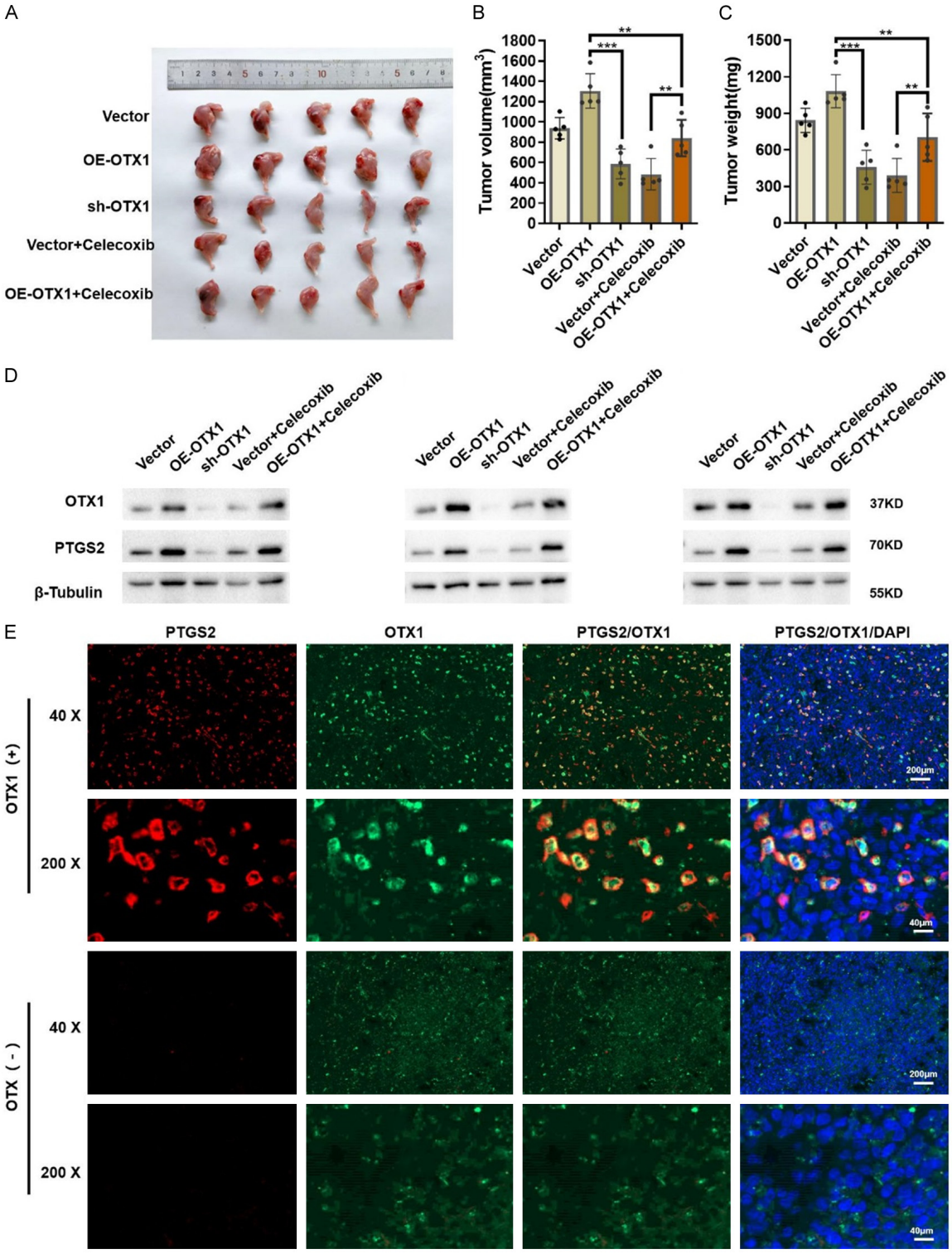

Figure 6. OTX1 knockdown or PTGS2 inhibitor suppresses OS growth in vivo. A. 8-weeks-old female BALB/c nude mice orthotopically injected with the indicated cell into tibial plateau, with the primary tumor volume measured every three days. B, C. Measurement of tumor volume and tumor weight post-sacrifice. D. OTX1 and PTGS2 protein expression detected in mouse model tissue by Western blot. E. Co-expression of OTX1 and PTGS2 in OS samples detected by multiplex immunofluorescence staining. Tumor volumes were analyzed by twoway repeated measures ANOVA (group × time), followed by Bonferroni's post-hoc test for intergroup comparisons at each time point. Tumor weights were analyzed by multifactor ANOVA. **P < 0.01, ***P < 0.001. Error bars represent mean ± SD. Scale bars, 40 μm and 200 μm.

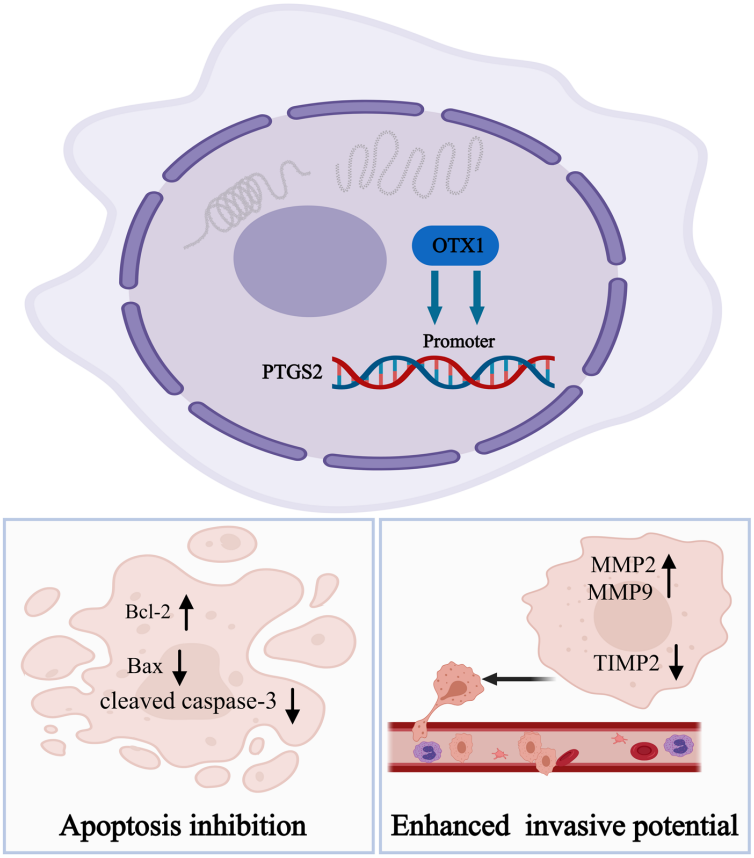

Figure 7. Schematic illustration of OTX1-mediated malignant phenotype in OS.

present research group further demonstrate that the downstream effects of the OTX1-PTGS2 axis operate in a "two-pronged" manner. On one hand, it confers robust anti-apoptotic capability to cells by upregulating Bcl-2, inhibiting Bax function, and reducing cleaved caspase-3 levels. On the other hand, it significantly enhances cellular migratory and invasive potential by upregulating MMP2/MMP9 and downregulating their inhibitor TIMP2. This mechanism - simultaneously enhancing both "survival fitness" and "mobility" - offers a direct molecular explanation for the heightened tendency toward recurrence and metastasis observed in patients with high OTX1 expression. Such cells exhibit not only increased resistance to elimination by conventional therapies but also greater capacity for distant dissemination.

theoretical foundation for developing therapeutic strategies targeting this signaling axis.

This study first establishes the oncogenic relevance of OTX1 at the clinical level. OTX1 is significantly overexpressed in OS tissues and closely associated with poor patient overall survival and progression-free survival. This clinical observation is strongly corroborated by functional experiments. OTX1 markedly promotes the proliferation, migration, and invasion of OS cells in vitro, while accelerating tumor growth in vivo. Most importantly, the core finding of this study identifies PTGS2 as the key downstream effector mediating OTX1-driven malignancy. Through transcriptomic screening, ChIP-PCR, and reporter gene assays, OTX1 is verified to bind to a specific site on the PTGS2 promoter and activate its transcription. PTGS2, as the rate-limiting enzyme for prostaglandin E2 (PGE2) synthesis, serves as a critical node linking inflammation and cancer [18]. Subsequent experiments by the

PTGS2 (COX-2) has been extensively documented to be aberrantly overexpressed in various solid tumors, including gastric cancer, pancreatic cancer, prostate cancer, and melanoma. It promotes tumor progression by regulating multiple signaling pathways involved in cell proliferation, angiogenesis, apoptosis resistance, invasion, metastasis, and immune suppression. For example, in gastric cancer, Harmine can induce apoptosis and inhibit tumor proliferation, migration, and invasion by downregulating COX-2 expression, upregulating the pro-apoptotic protein Bax, and simultaneously suppressing the anti-apoptotic protein BCL-2 and the invasion-related protein MMP2 [19]. In colorectal cancer, RUNX1 upregulates PTGS2, thereby promoting MMP9 overexpression; this drives cancer cell growth, migration, and invasion [20]. Furthermore, the COX-2 inhibitor celecoxib has been shown to downregulate the MMP2/TIMP2 ratio and MMP-9 expression in colorectal cancer, exerting anti-angiogenic and pro-apoptotic effects, demonstrating targeting

COX-2 as a promising therapeutic strategy for cancer [21]. In OS, studies have reported that the oncogene PAFAH1B3 can maintain high PTGS2 expression, facilitating cell cycle transition from G_1 to S phase and thereby accelerating cell proliferation [22]. Nonetheless, the upstream transcriptional regulatory mechanisms of PTGS2 in OS remain incompletely understood. This study reveals that OTX1 positively regulates PTGS2 expression in OS cells and mice xenograft models. Results indicate that OTX1 may serve as a novel transcriptional regulator of PTGS2 in OS, providing a fresh mechanistic perspective on the aberrant expression of PTGS2 in this malignancy.

This series of discoveries carries clear translational potential. First, OTX1 and PTGS2 may function as complementary prognostic biomarkers. IHC detection of OTX1/PTGS2 in tumor tissues from newly diagnosed patients can facilitate to identify a "high-risk subgroup" with intrinsically high metastatic potential and apoptosis resistance. Even following standard therapy, such patients may require closer follow-up monitoring or consideration of more intensive adjuvant strategies. Second, the current study provides prospective experimental evidence for the drug repurposing of COX-2 inhibitors. Celecoxib, a non-steroidal anti-inflammatory drug already widely used in the clinic, features a relatively well-established safety profile. The present findings suggest that for OS with high OTX1/PTGS2 expression, celecoxib could serve as a potential adjuvant or maintenance treatment option, aiming to delay recurrence and reduce metastasis by inhibiting PTGS2 activity. While long-term use requires weighing cardiovascular risks, time-limited dosing or localized delivery strategies in the oncology setting may circumvent this concern. Finally, while OTX1 - by virtue of its role as a transcription factor - is challenging to target directly, interventions aimed at its upstream regulators or downstream PGE2 receptors emerge as promising directions for future drug development.

However, this study still has certain limitations. The clinical sample size warrants further validation in larger cohorts to confirm the prognostic value of OTX1/PTGS2. Despite the encouraging efficacy of celecoxib in animal models, its effectiveness in OS patients, optimal dosing schedule, and potential synergies with existing chemotherapy regimens should still be further evaluated through rigorous clinical trials. Moreover, the upstream mechanisms leading to aberrant OTX1 activation in OS, such as epigenetic regulation or upstream signaling pathways, remain unelucidated and represent an important direction for future research.

Conclusion

In summary, this study reveals the pivotal oncogenic role and molecular mechanism of transcription factor OTX1 in OS. OTX1 directly binds to and transcriptionally activates the PTGS2 gene. It thus modulates downstream apoptotic (Bcl-2/Bax/caspase-3) and invasive (MMP2/MMP9/TIMP2) protein networks, synergistically promoting OS cell proliferation, anti-apoptosis, migration, and invasion. The activation of this OTX1/PTGS2 signaling axis has been corroborated across cellular models, in vivo animal experiments, and clinical samples. Furthermore, pharmacological inhibition of PTGS2 activity effectively reverses the tumor-promoting effects of OTX1. Collectively, these findings provide a novel theoretical framework informing the malignant progression of OS, particularly in high-risk subgroups prone to recurrence and metastasis, and open innovative translational avenues for improving the clinical prognosis of OS patients.

Acknowledgements

This work was supported by the National Natural Science Foundation of China under Grant Number (82305057, 82573785, 82273363).

Disclosure of conflict of interest

None.

Address correspondence to: Drs. Tielong Liu and Xinghai Yang, Department of Orthopaedic Oncology, The Second Affiliated Hospital of Naval Medical University, 415 Fengyang Road, Shanghai 200003, China. E-mail: czyyltl@smmu.edu.cn (TLL); cnspineyang@163.com (XHY); Dr. Zhitao Han, School of Integrated Chinese and Western Medicine, Nanjing University of Chinese Medicine, 138 Xianlin Avenue, Nanjing 210023, Jiangsu, China. E-mail: 290517@njucm.edu.cn

References

[1] Wen Y, Tang F, Tu C, Hornicek F, Duan Z and Min L. Immune checkpoints in osteosarcoma: recent advances and therapeutic potential. Cancer Lett 2022; 547: 215887.

[2] Bishop MW. Osteosarcoma: diagnosis, treatment, and emerging opportunities. Hematol Oncol Clin North Am 2025; 39: 749-760.

[3] Goorin AM, Harris MB, Bernstein M, Ferguson W, Devidas M, Siegal GP, Gebhardt MC, Schwartz CL, Link M and Grier HE. Phase II/III trial of etoposide and high-dose ifosfamide in newly diagnosed metastatic osteosarcoma: a pediatric oncology group trial. J Clin Oncol 2002; 20: 426-433.

[4] Davis LE, Bolejack V, Ryan CW, Ganjoo KN, Loggers ET, Chawla S, Agulnik M, Livingston MB, Reed D, Keedy V, Rushing D, Okuno S, Reinke DK, Riedel RF, Attia S, Mascarenhas L and Maki RG. Randomized double-blind phase II study of regorafenib in patients with metastatic osteosarcoma. J Clin Oncol 2019; 37: 1424-1431.

[5] Xie L, Xu J, Sun X, Tang X, Yan T, Yang R and Guo W. Apatinib for advanced osteosarcoma after failure of standard multimodal therapy: an open label phase II clinical trial. Oncologist 2019; 24: e542-e550.

[6] Gaspar N, Campbell-Hewson Q, Gallego Melcon S, Locatelli F, Venkatramani R, Hecker-Nolting S, Gambart M, Bautista F, Thebaud E, Aerts I, Morland B, Rossig C, Canete Nieto A, Longhi A, Lervat C, Entz-Werle N, Strauss SJ, Marec-Berard P, Okpara CE, He C, Dutta L and Casanova M. Phase I/II study of single-agent lenvatinib in children and adolescents with refractory or relapsed solid malignancies and young adults with osteosarcoma (ITCC-050) (☆). ESMO Open 2021; 6: 100250.

[7] Gupta S, Ito T, Alex D, Vanderbilt CM, Chang JC, Islamdoust N, Zhang Y, Nafa K, Healey J, Ladanyi M and Hameed MR. RUNX2 (6p21.1) amplification in osteosarcoma. Hum Pathol 2019; 94: 23-28.

[8] Weekes D, Kashima TG, Zandueta C, Perurena N, Thomas DP, Sunters A, Vuillier C, Bozec A, El-Emir E, Miletich I, Patiño-Garcia A, Lecanda F and Grigoriadis AE. Regulation of osteosarcoma cell lung metastasis by the c-fos/AP-1 target FGFR1. Oncogene 2016; 35: 2852-2861.

[9] Yang C, Chen Y, Tang G, Shen T and Li L. Dysregulation of c-jun (JUN) and FBJ murine osteosarcoma viral oncogene homolog B (FOSB) in obese people and their predictive values for metabolic syndrome. Endocr J 2024; 71: 1157-1163.

[10] Gu W, Zhang E, Song L, Tu L, Wang Z, Tian F, Aikenmu K, Chu G and Zhao J. Long noncoding RNA HOXD-as1 aggravates osteosarcoma carcinogenesis through epigenetically inhibiting p57 via EZH2. Biomed Pharmacother 2018; 106: 890-895.

[11] Pantò MR, Zappalà A, Tuorto F and Cicirata F. Role of the Otx1 gene in cell differentiation of mammalian cortex. Eur J Neurosci 2004; 19: 2893-2902.

[12] Cao B, Liu K, Tian C, He H, He S, Chen H, Zhang X, Liu Y, Wang L, Liu X, Li M, Jia Q and Chai J. OTX1 regulates tumorigenesis and metastasis in glioma. Pathol Res Pract 2024; 254: 155116.

[13] Li H, Miao Q, Xu C, Huang J, Zhou Y and Wu MJ. OTX1 contributes to hepatocellular carcinoma progression by regulation of ERK/MAPK pathway. J Korean Med Sci 2016; 31: 1215-1223.

[14] Qin SC, Zhao Z, Sheng JX, Xu XH, Yao J, Lu JJ, Chen B, Zhao GD, Wang XY and Yang YD. Dowregulation of OTX1 attenuates gastric cancer cell proliferation, migration and invasion. Oncol Rep 2018; 40: 1907-1916.

[15] Hashemi Goradel N, Najafi M, Salehi E, Farhood B and Mortezaee K. Cyclooxygenase-2 in cancer: a review. J Cell Physiol 2019; 234: 5683-5699.

[16] Ye Y, Wang X, Jeschke U and von Schönfeldt V. COX-2-PGE(2)-EPs in gynecological cancers. Arch Gynecol Obstet 2020; 301: 1365-1375.

[17] Chen H, Qian Z, Zhang S, Tang J, Fang L, Jiang F, Ge D, Chang J, Cao J, Yang L and Cao X. Silencing COX-2 blocks PDK1/TRAF4-induced AKT activation to inhibit fibrogenesis during skeletal muscle atrophy. Redox Biol 2021; 38: 101774.

[18] Martín-Vázquez E, Cobo-Vuilleumier N, López-Noriega L, Lorenzo PI and Gauthier BR. The PTGS2/COX2-PGE(2) signaling cascade in inflammation: pro or anti? A case study with type 1 diabetes mellitus. Int J Biol Sci 2023; 19: 4157-4165.

[19] Zhang H, Sun K, Ding J, Xu H, Zhu L, Zhang K, Li X and Sun W. Harmine induces apoptosis and inhibits tumor cell proliferation, migration and invasion through down-regulation of cyclooxygenase-2 expression in gastric cancer. Phytomedicine 2014; 21: 348-355.

[20] Zheng W, Guo Y, Kahar A, Bai J, Zhu Q, Huang X, Li Y, Xu B, Jia X, Wu G, Zhang C and Zhu Y. RUNX1-induced upregulation of PTGS2 enhances cell growth, migration and invasion in colorectal cancer cells. Sci Rep 2024; 14: 11670.

[21] Gungor H, Ilhan N and Eroksuz H. The effectiveness of cyclooxygenase-2 inhibitors and evaluation of angiogenesis in the model of experimental colorectal cancer. Biomed Pharmacother 2018; 102: 221-229.

[22] Fan J, Yang Y, Qian JK, Zhang X, Ji JQ, Zhang L, Li SZ and Yuan F. Aberrant expression of PAFAH1b3 affects proliferation and apoptosis in osteosarcoma. Front Oncol 2021; 11: 664478.

Supplementary Table 1. Primer for PCR or single-stranded DNA for anneal

Name	Sequence
OTX1-F	AAACAACCCCCATACGGCAT
OTX1-R	ACTCCGGCAGGTTGATCTTG
PTGS2-S1-F	CTCACCCTCACATGCTCCTC
PTGS2-S1-R	TGAGTTGTGACCATGGATCAA
PTGS2-S2-F	AGTGAACTTTAAAACTCGAA
PTGS2-S2-R	TGGTCCTAAGCAGTTACCCTG
ALPP-S1-F	AGTAGAGATGGGGATTATCC
ALPP-S1-R	GAGTGGCAAGGGCTGTTGCC
ALPP-S2-F	AGGCTGAGGCAGGAGGATCAC
ALPP-S2-R	GAGGCAGGGTCTCATTTGTC

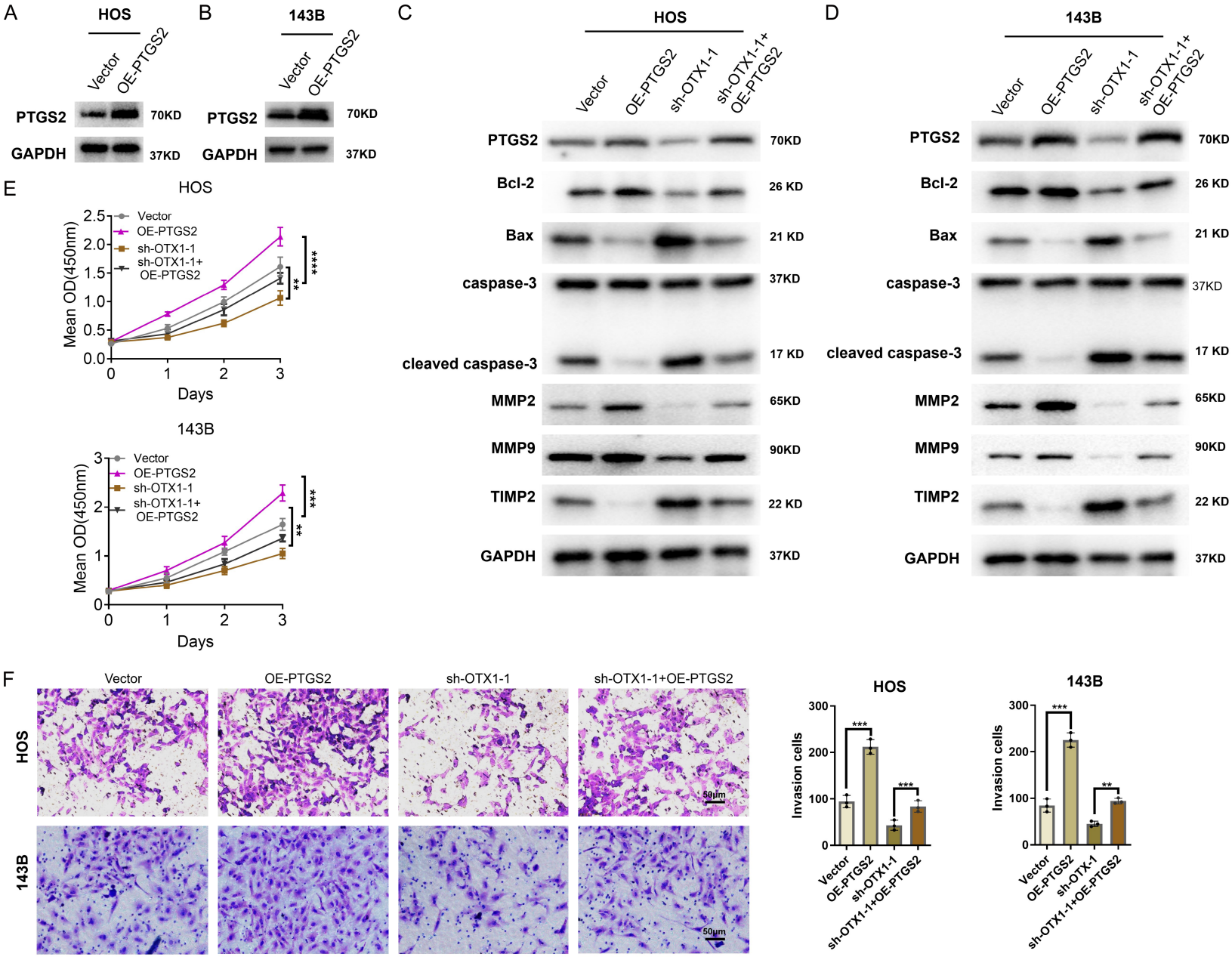
A
HOS
Vector
OE-PTGS2
PTGS2
70KD
GAPDH
37KD
B
143B
Vector
OE-PTGS2
PTGS2
70KD
GAPDH
37KD
C
HOS
Vector
OE-PTGS2
sh-OTX1-1
sh-OTX1-1+ OE-PTGS2
PTGS2
70KD
Bcl-2
26 KD
Bax
21 KD
caspase-3
37KD
cleaved caspase-3
17 KD
MMP2
65KD
MMP9
90KD
TIMP2
22 KD
GAPDH
37KD
D
143B
Vector
OE-PTGS2
sh-OTX1-1
sh-OTX1-1+ OE-PTGS2
PTGS2
70KD
Bcl-2
26 KD
Bax
21 KD
caspase-3
37KD
cleaved caspase-3
17 KD
MMP2
65KD
MMP9
90KD
TIMP2
22 KD
GAPDH
37KD
E
HOS
Mean OD(450nm)
Days
Vector
OE-PTGS2
sh-OTX1-1
sh-OTX1-1+ OE-PTGS2
143B
Mean OD(450nm)
Days
Vector
OE-PTGS2
sh-OTX1-1
sh-OTX1-1+ OE-PTGS2
F
Vector
OE-PTGS2
sh-OTX1-1
sh-OTX1-1+OE-PTGS2
HOS
143B
50μm
50μm
HOS
Invasion cells
Vector
OE-PTGS2
sh-OTX1-1
sh-OTX1-1+OE-PTGS2
143B
Invasion cells
Vector
OE-PTGS2
sh-OTX1-1
sh-OTX1-1+OE-PTGS2

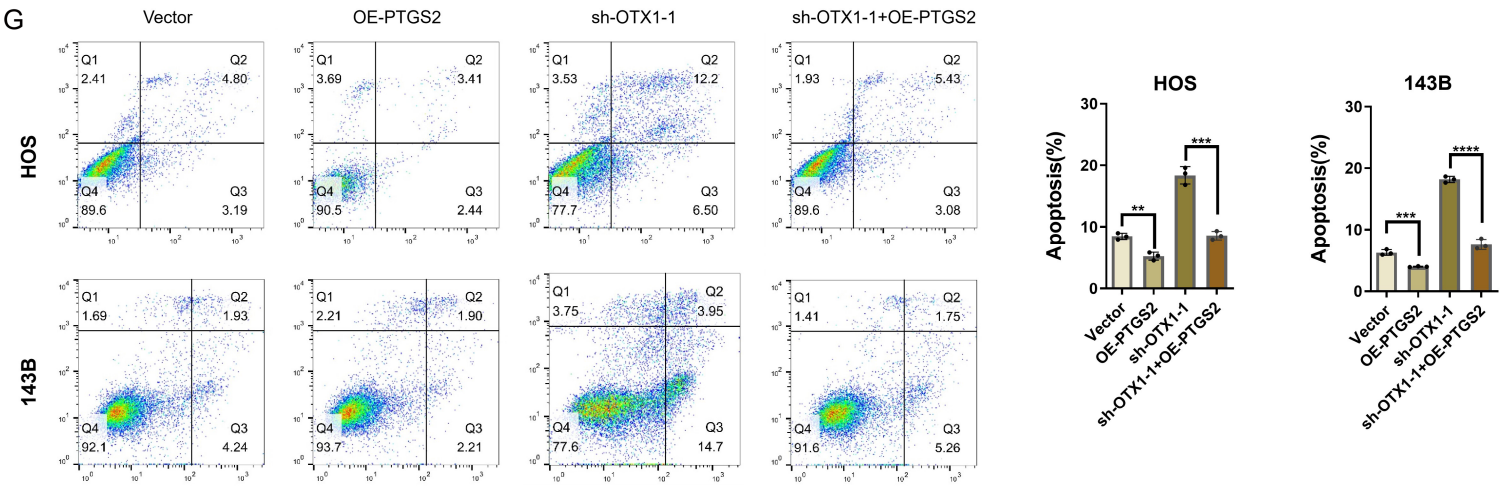

Supplementary Figure 1. Overexpression of PTGS2 in OTX1-knockdown cells and assessment of related phenotypes. (A, B) Western blot analysis of PTGS2 transfection efficiency in OTX1-knockdown cells. (C, D) Western blots were performed to detect the expression levels of Bcl-2, Bax, caspase-3, cleaved caspase-3, MMP2, MMP9, and TIMP2 in the indicated OS cells. (E) Cell proliferation activity of the indicated groups was measured by CCK-8 assay. (F) The effect of PTGS2 overexpression on the migration ability of OTX1-knockdown cells was evaluated by Transwell assay. (G) The effect of PTGS2 on apoptosis of OTX1-knockdown cells was assessed using flow cytometry. Statistical analysis were performed using two-way repeated measures ANOVA with Bonferroni's post-hoc test (E) and multifactor ANOVA (F, G). Error bars show means ± SD. **P < 0.01, ***P < 0.001, ****P < 0.0001. Scale bars, 50 μm.